Available online at www.sciencedirect.com
ScienceDirect
Ceramics International 36 (2010) 1347–1355
CERAMICS INTERNATIONAL
www.elsevier.com/locate/ceramint

Preparation, characterization, photoactivity and XPS studies of Ln_2ZrTiO_7 (Ln = Sm and Nd)

B. Vijaya Kumar [a], Radha Velchuri [a], G. Prasad [b], B. Sreedhar [c], K. Ravikumar [d], M. Vithal [a,*]

[a] Department of Chemistry, Osmania University, Hyderabad-500 007, India
[b] Department of Physics, Osmania University, Hyderabad-500 007, India
[c] Inorganic and Physical Chemistry Division, Indian Institute of Chemical Technology, Hyderabad-500 007, India
[d] Laboratory of X-ray Crystallography, Indian Institute of Chemical Technology, Hyderabad-500 007, India

Received 15 October 2009; received in revised form 4 December 2009; accepted 4 January 2010
Available online 1 February 2010

Abstract

Oxides of composition Ln_2ZrTiO_7 (Ln = Sm and Nd) were prepared by sol–gel method and characterized by powder X-ray diffraction (XRD), energy dispersive spectra (EDS), Raman, X-ray photoelectron spectroscopy (XPS), transmission electron microscopy (TEM) and scanning electron microscopy (SEM). These compounds were crystallized in the disordered pyrochlore structure in cubic lattice with $Fd\bar{3}m$ space group. The TEM images of Sm_2ZrTiO_7 and Nd_2ZrTiO_7 prepared at 600 °C gave the particle size of 13 and 21 nm respectively. The photocatalytic activity of products was studied using photodegradation of methyl orange under UV light irradiation. The photocatalytic activity of these oxides was found to be less than that of $La_2Zr_2O_7$ and $Nd_2Zr_2O_7$. The 3d profile of Nd_2ZrTiO_7 gave satellite peaks on the low binding energy side in the XPS spectrum which were absent in the XPS spectrum of Sm_2ZrTiO_7. The reasons for the observation of satellite peaks were given.

Keywords: Sol–gel; Transmission electron microscopy; Powder XRD; Photocatalytic activity

1. Introduction

Oxide materials exhibiting pyrochlore structure have attracted scientific and industrial community due to their interesting properties and potential applications. These compounds have high photocatalytic activity, piezoelectric behavior, ferro- and ferrimagnetisms, order/disorder transformations, high thermal expansion coefficient, range of electrical and ionic conductivities that include metallic, semiconducting and superconductivity [1–7]. Due to these combinations of properties they are used as magnetic materials [8,9], as fast ion conductors [10–13], as thermal barrier coating materials in gas turbines [7] and in the immobilization and treatment of nuclear waste [14,15]. The general formula of pyrochlore oxides is $A_2B_2O_7$ or $A_2B_2O_6O'$ or $B_2O_6A_2O'$. The structure is characterized by corner shared BO_6 octahedra forming a B_2O_6 network which intersects with A–O′ chains of formula A_2O' [1]. Further, defects can occur in the A_2O' network. The site A can be occupied by trivalent rare earth or divalent alkaline earth or monovalent alkali ions. Tetra, penta or hexavalent transition metal ions occupy the site B. Thus the structure is flexible for substitution at A or B sites giving rise to a large family of materials.

The studies on materials containing rare earth ions are interesting. The 4f levels in rare earth ions (except Ce) are strongly localized within the ion and does not contribute significantly to chemical bonding although Mott-type phase transition of Pr in metallic systems under pressure is an exception [16,17]. The coupling of 4f states with delocalized electrons, the number of electrons present in 4f orbitals (the so called *f* count) and the possibility of hybridization has been the subject of many investigations [18–25]. The observation of satellite peaks for 3d core level in the XPS spectra of some rare earth ions, their origin and variation of their intensity with respect to main peaks has made these rare earth materials attractive both from experimental and theoretical points of view. The present investigation is aimed at the preparation, characterization, XPS and photocatalytic studies of new nano sized Sm_2ZrTiO_7 and Nd_2ZrTiO_7.

* Corresponding author. Tel.: +91 40 27682337; fax: +91 40 27090020.
E-mail address: muga_vithal@osmania.ac.in (M. Vithal).

0272-8842/$36.00
doi:10.1016/j.ceramint.2010.01.019

2. Experimental

Rare earth oxide (Ln_2O_3, Ln = Sm and Nd) (Indian Rare Earths Ltd., purity 99%), zirconyl nitrate (Wilson Laboratories, Bombay), Ti (100 mesh, Aldrich 99.7%), H_2O_2 (30%, SD Fine) and ammonia solution (25%, AR grade, SD Fine) were used as received.

Solution "A". Stoichiometric amount of Ln_2O_3 was dissolved in excess of concentrated nitric acid to form rare earth nitrate. Excess nitric acid was removed by slow heating. About 25 ml of distilled water was added. This solution contains 11.12 mmol of Ln^{3+} ions.

Solution "B". Calculated amount of zirconyl nitrate was dissolved in hot water. The solution contains 5.56 mmol of Zr^{4+} ions.

Solution "C". Calculated amount of Ti powder was added to a solution containing 60 ml of H_2O_2 and 10 ml of ammonia at 0–10 °C under constant stirring. A yellow gel was obtained after 6 h. The solution contains 5.56 mmol of Ti^{4+} ions.

Solution "A" was mixed with solution "B". To this resultant solution, solution "C" was added. Then citric acid was added to this solution such that the molar ratio of citric acid:metal ion is 2:1. At this stage metal citrates are believed to be formed. The total volume of the solution was about 300 ml. The pH of the resultant metal citrate solution was adjusted to 6–7 by adding dilute ammonia solution drop wise. The solution was then slowly evaporated on a water bath till a viscous liquid was obtained. At this stage ethylene glycol (gelating reagent) was added such that the molar ratio of citric acid to ethylene glycol was 1:1.2. This mixture was heated on a hot plate/stirrer at 100 °C for 2–3 h with constant stirring. The temperature was increased to 160–180 °C at the onset of solidification. The ensuing porous solid mass was ground in an agate mortar using spectral grade acetone and heated to about 400 °C in small amounts in an electric burner to remove the organic matter completely. The resultant ash colored solid (named as "precursor") was mixed with solid NaCl in the weight ratio of 1:1 and divided into several parts.

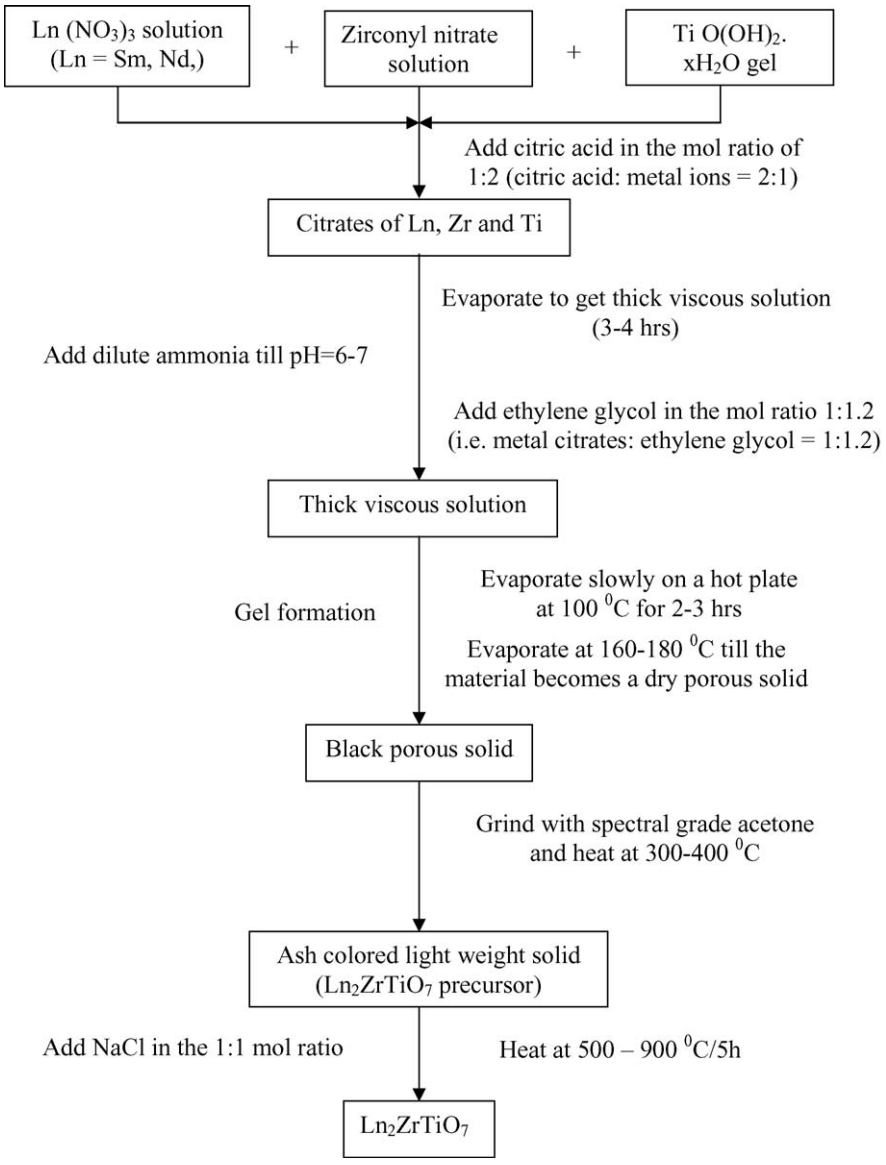

Fig. 1. Flow chart showing the sol–gel method of preparation of Ln_2ZrTiO_7.

Each part was heated in a muffle furnace at various temperatures (500–900 °C) for 5 h to obtain the desired pyrochlore oxide (hereafter named as SZT (Sm_2ZrTiO_7) and NZT (Nd_2ZrTiO_7)). The addition of NaCl to precursor solid is to prevent the process of agglomeration [26]. The steps involved in this process are shown as flow chart in Fig. 1.

The powder X-ray diffractograms were recorded on Siemens D-5000 powder X-ray diffractometer using Cu-Kα radiation of wavelength 1.5406 Å. The step size was 0.005? and step time was 10.3 s. Raman spectra were recorded using a 632.81 nm line from a He–Ne laser and the scattered light was analyzed using HORIBA JOBIN YVON HR800. The laser was focused on a spot of ~3 μm and a 10× lens was used for the collection of back scattered Raman signal. Transmission electron microscopy (TEM) images were recorded on a TECNAI FE1 FE12 transmission electron microscope and SEM-EDS images were recorded on the HITACHI SU-1500 variable pressure scanning electron microscope (VP-SEM). X-ray photoelectron spectroscopic (XPS) measurements were performed on a KRATOS AXIS165 X-ray photoelectron spectrometer. Using excitation energy of 1253.6 eV (Mg KR), the spectra were recorded with pass energy of 80 eV. The photoreactivities of the samples were evaluated by methyl orange decomposition under UV irradiation. The initial concentration of methyl orange in a quartz round-bottomed flask was fixed at 20 mg/L with catalysts loading of 1 g/L. The extent of methyl orange decomposition was determined by measuring the absorbance at 465 nm on UVIKON 923 UV-Vis spectrophotometer.

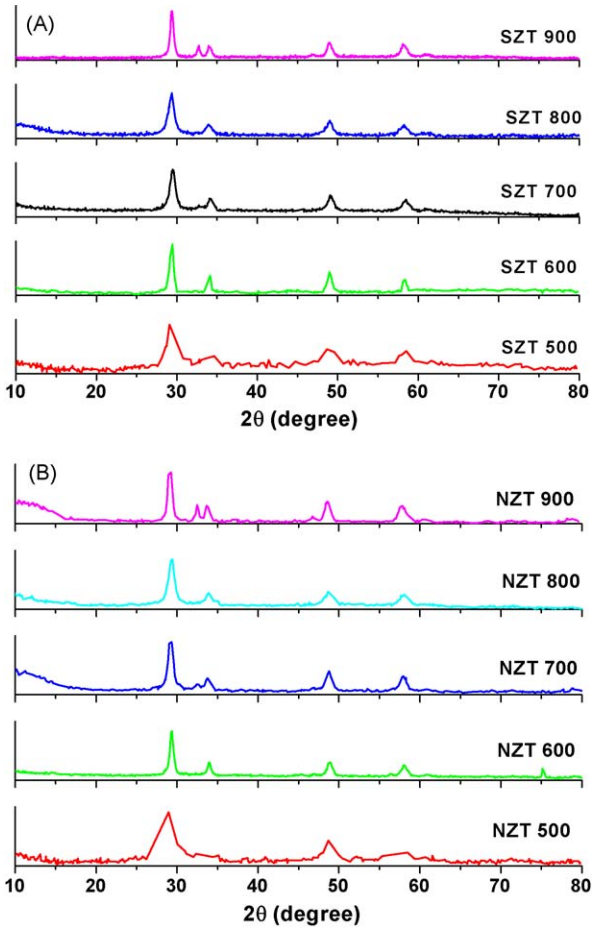

Fig. 2. Powder XRD of (A) SZT and (B) NZT.

3. Results and discussion

3.1. Powder XRD

The room temperature powder X-ray diffraction patterns of SZT and NZT prepared in the temperature range 500–900 °C are shown in Fig. 2. These powder XRDs are similar to the powder XRDs of $La_2Zr_2O_7$ and $RE_2Hf_2O_7$ (RE = Dy, Ho, Er, Tm, Lu and Y) [27,28] and free from unreacted reactants or impurities. The *d*-values obtained from the powder XRD patterns for samples heated at 900 °C and the unit cell parameters of $La_2Zr_2O_7$ are given as input values and least square fitted using POWD software. Both the samples are found to be isomorphous with the $La_2Zr_2O_7$ [28] and found to crystallize in cubic lattice with $Fd\bar{3}m$ space group [29]. However, typical super lattice peaks at $2\theta \approx 14°$, 27°, 36° and 50° normally observed for pyrochlore lattice are absent in these two materials. It is observed that the phase in which $A_2B_2O_7$ crystallizes depends on (a) the relative ionic size ratio of A and B cations and (b) sample processing conditions [27,30,31]. The pyrochlore oxides were found to be stable when the radius ratio (r_A/r_B) of the cations lies within the range 1.46–1.78 [32]. Mandal et al. have reported this radius ratio as 1.2–1.6 [27]. Oxides of general formula $A_2B_2O_7$ crystallize in ordered pyrochlore (cubic, $Fd\bar{3}m$) and defect fluorite (cubic, $Fm3m$) structures when the radius ratio (r_A/r_B) is in the lower and upper limits of the above range respectively. Further, Glerup et al. have noticed the certain $A_2B_2O_7$ type oxides also adopt 'disordered pyrochlore' structure within the above two limits [33]. It should be noted that the numerical value of radius ratio r_A/r_B should be used only as a broad guideline in view of some exceptions [31]. As the radius increases from the lower limit, pyrochlore super structure peaks at $2\theta \approx 14°, 27°, 36°, 50°$, etc. (for Cu-$K_\alpha$ source) corresponding to (1 1 1), (3 1 1), (3 3 1), (5 3 1) planes respectively will appear [27]. In the present investigation the radius ratio (r_A/r_B) was found to be Sm/Zr = 1.50, Sm/Ti = 1.77, Nd/Zr = 1.55 and Nd/Ti = 1.83. These values are on the higher side of the above range. Therefore, both these samples are expected to crystallize in the ordered pyrochlore structure. But the absence of super structure *d*-lines at $2\theta \approx 14°$, 27°, 36°, 50° in NZT and SZT suggests that these materials may have defect fluorite or disordered pyrochlore structure. Dickson et al. have shown that the intensity of (1 1 1) reflection is most sensitive to the fractional coordinate, *x* (or *x*-parameter) of 48f oxygen in $A_2B_2O_7$ oxides [34]. The *x*-parameter is found to be in the range 0.3125–0.375 in these oxides. The lower and upper limits of this range correspond to 'ordered pyrochlore' and 'defect fluorite' structures respectively. It is observed that at $x = 0.3125$, B cation adopts a perfect octahedral coordination and A cation is at the centre of distorted hexagonal network of six 48f oxygen with two oxygen (8b O′) perpendicular to hexagonal plane. At $x = 0.375$, BO_6 octahedron is highly distorted and "A" cation occupies the

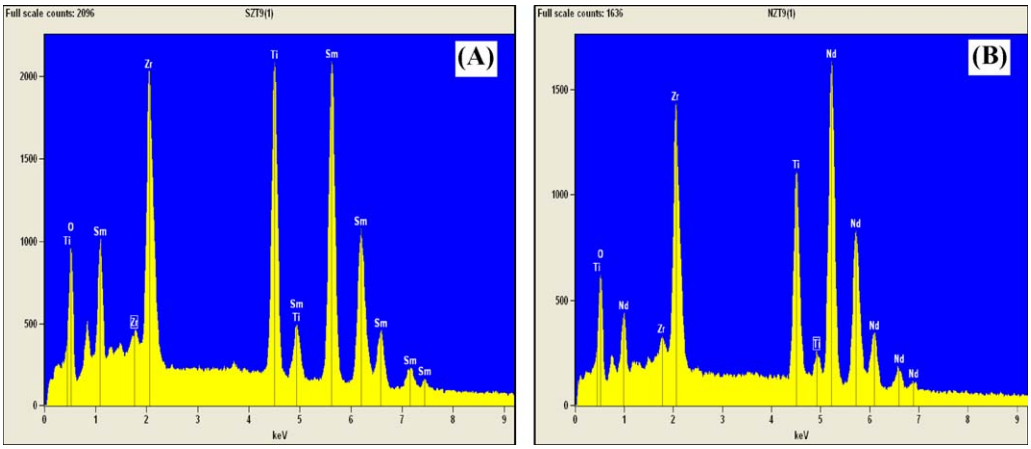

Fig. 3. EDS of (A) SZT and (B) NZT.

centre of regular cube [35]. The intensity of (1 1 1) reflection decreases to zero as the *x*-parameter approaches the 'defect fluorite' limit (i.e. 0.375) [34]. Mandal et al. [27] have reported that $Dy_2Hf_2O_7$ crystallizes in "disordered pyrochlore" structure in spite of the absence of super structure *d*-lines at $2\theta \approx 14^\circ, 27^\circ, 36^\circ, 50^\circ$. These super structure lines were not observed by laboratory X-ray diffractometer due to their low intensity. In the present investigation, we believe that both SZT and NZT have crystallized in "disordered pyrochlore" structure in spite of the absence of super structure *d*-lines. The crystallite size of the SZT and NZT powders was calculated from the broadening in their respective XRD peaks using the Scherer formula [36].

$$t = \frac{0.9\lambda}{B\cos\theta}$$

where "*t*" is the thickness in Angstroms (Å) and corresponds to the diameter of particles assuming spherical shape, "λ" is the wavelength of the X-rays used, "θ" is the Bragg angle, and "*B*" is the full width at half maximum measured in radians of the most intense line in the X-ray diffractogram. The crystallite size of both the samples prepared at 500 °C was found to be ≈20 nm while it increased to ≈40 nm for samples prepared at 900 °C. It is generally observed that for samples prepared by gel burning method, the crystallite size increases with increase in the temperature of sintering due to enhanced nucleation and growth.

3.2. EDS analysis

The energy dispersive spectra (EDS) of samples prepared at 900 °C are shown in Fig. 3. The area ratio of Ln, Zr and Ti was found to be close to 2:1:1 confirming the molecular formula as Ln_2ZrTiO_7.

3.3. Raman spectra

It is well known that Raman spectroscopic investigation gives unequivocal information to identify the structure of $A_2B_2O_7$ materials [33]. Therefore, the Raman spectra of both SZT and NZT are recorded. The Raman spectra of $A_2B_2O_7$ give characteristic bands depending on the structure adopted by these oxides. According to factor group analysis, $A_2B_2O_7$ gives six Raman active modes of vibrations if it adopts ordered pyrochlore structure viz.,

$$\Gamma = A_{1g} + E_g + 4F_{2g} \quad (1)$$

On the other hand, $A_2B_2O_7$ oxides with fluorite structure give only one Raman active mode viz.,

$$\Gamma = F_{2g} \quad (2)$$

The Raman spectra of SZT and NZT are shown in Fig. 4. The assignment of Raman peaks to different modes of vibrations (Eq. (1)) is difficult in the absence of polarized Raman spectra. The similarity of Raman spectra observed in the present investigation with those reported suggests that these materials have crystallized in "pyrochlore" structure. The assignment of Raman peaks in the present investigation is made by comparing the Raman bands in different similar systems where valence force field calculations were carried out to interpret the results [33,37,38]. The most intense peak observed at 313 cm^{-1} was assigned to E_g while less intense peaks at 216 (275), 446 (424) and 609 (565) (the peak positions given in the parentheses correspond to NZT) were assigned to three of the four F_{2g}

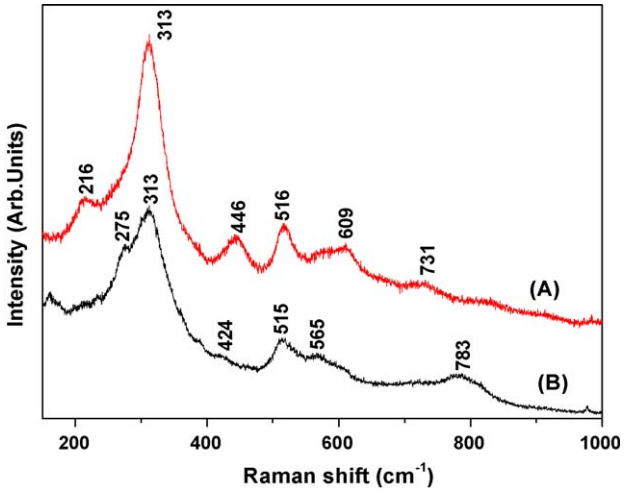

Fig. 4. Raman spectra of (A) SZT and (B) NZT.

Table 1
Raman peak positions and their assignments of Ln_2ZrTiO_7 along with the peak positions of related systems.

$Gd_2Ti_2O_7$ [39]	Gd_2ZrTiO_7 [39]	Sm_2ZrTiO_7 (this work)	Nd_2ZrTiO_7 (this work)	Assignment
519	522	516	515	A_{1g}
312	307	313	313	E_g
219	220	216	275	F_{2g}
455	–	446	424	F_{2g}
549	572	609	565	F_{2g}
–	–	731	783	Overtone

modes. The band at 516 (515) was assigned to A_{1g} mode. The band observed at 731 (783) cm^{-1} may be assigned to an overtone as reported earlier [39]. In the case of NZT the peaks at 275 and 313 are fitted to two Lorentzian. Table 1 gives the Raman peak positions and their assignments of SZT and NZT along with the peak positions of related systems [40]. The line widths of intense peak (E_g) for SZT and NZT were found to be ≈40 and ≈50 cm^{-1} respectively. The magnitude of these line widths is higher than the line width found for ordered pyrochlore structure. It is noticed that broad Raman lines arise due to inherent cation disorder in the structure and/or small particle size. In the present investigation, the relatively broad line width in the Raman spectra is attributed to both cation disorder and small particle size. The particle size of samples prepared at 900 °C was ≈40 nm (estimated from line width of powder XRD patterns using Scherrer's formula) for both SZT and NZT samples are in accordance with this view.

3.4. TEM and SEM

The structural and morphological characterization of SZT and NZT was carried out by TEM measurements. Figs. 5 and 6 show the TEM and selected area diffraction images of SZT and NZT (prepared at 600 °C/5 h) respectively. It is observed that both the samples have substantial agglomeration. The SAED image confirms the phase formation and absence of impurities. The morphology of SZT was found to be near spherical while the NZT particles were composed of spheres and platelet like objects. The average size of the particles measured from TEM figures was found to be 13 and 21 nm for SZT and NZT respectively prepared at 600 °C. These values are close to the values obtained from Scherrer's formula. The low magnification SEM images of SZT and NZT are shown in Fig. 7. The surface morphology of these samples is characterized by densely packed particles.

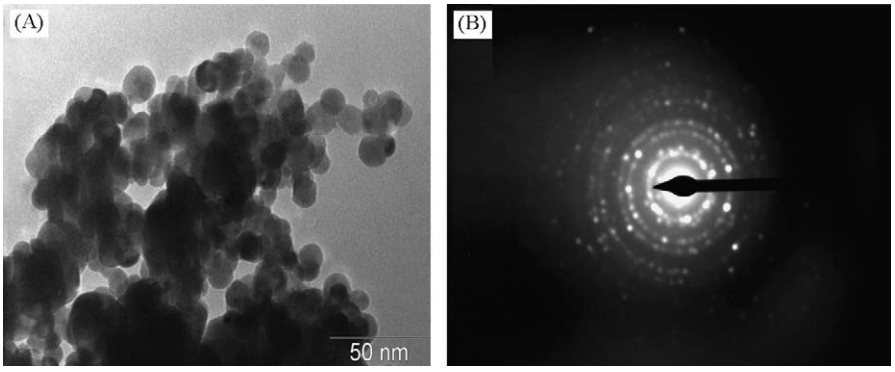

Fig. 5. (A) TEM and (B) selected area diffraction of SZT prepared at 600 °C/5 h.

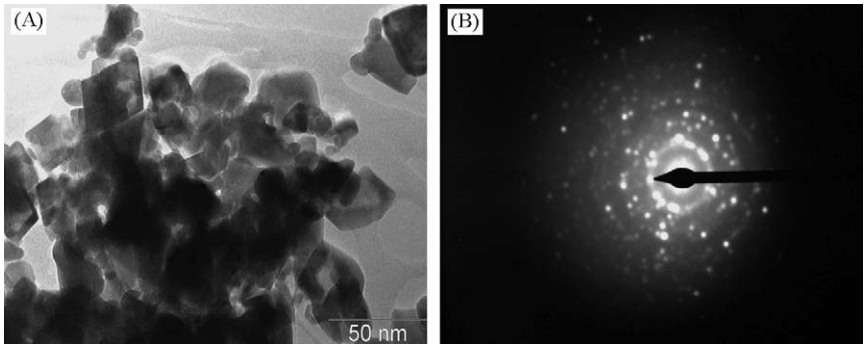

Fig. 6. (A) TEM and (B) selected area diffraction of NZT prepared at 600 °C/5 h.

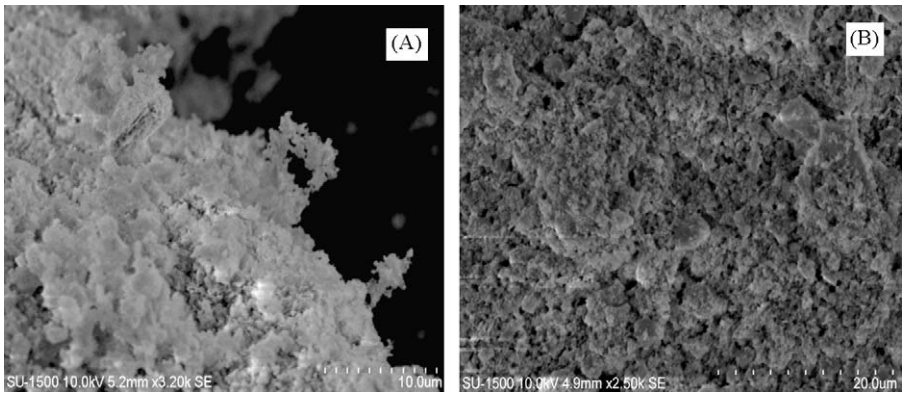

Fig. 7. SEM images of (A) SZT and (B) NZT.

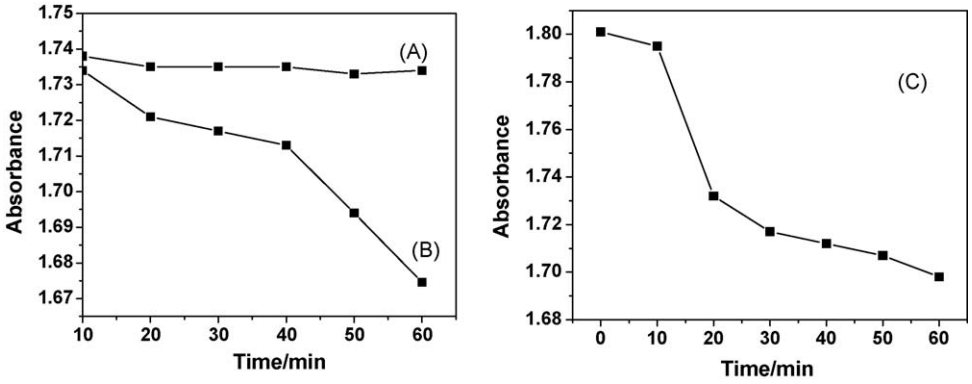

Fig. 8. Absorbance of methyl orange with time (A) without catalyst, (B) with SZT and (C) NZT.

3.5. Photocatalytic activity

Pyrochlore type of oxides exhibits the property of photoactivity. It is strongly influenced by the surface structure and nature of the material. High dispersibilty and large surface area of the materials are critically important to its catalytic behavior. The photocatalytic decomposition of methyl orange in the presence and absence of SZT and NZT is studied. Fig. 8 shows the absorbance of methyl orange in the presence and absence of Ln_2ZrTiO_7 as a function of time. It is noted that the concentration of methyl orange decreases with time in the presence of both the catalysts. The amount of methyl orange decomposed in the presence of these oxides was found to be <10% which is much lower compared to the photoactivity of $La_2Zr_2O_7$ and $Nd_2Zr_2O_7$ [41]. This may be due to nature of the materials and/or lower surface area due to agglomeration.

3.6. XPS studies

The XPS spectra of NZT and SZT are shown in Figs. 9 and 10 respectively. The spectra exhibit characteristic peaks due to Ln, Zr, Ti and O along with C 1s peak. The C 1s peak appears due to the contamination of organic compounds as the materials under investigation were prepared from ethylene glycol matrix. Fig. 10 shows the surface high resolution XPS spectrum of NZT. The XPS of NZT is characterized by Nd_{3d}, Zr_{3d}, Ti_{2p} and

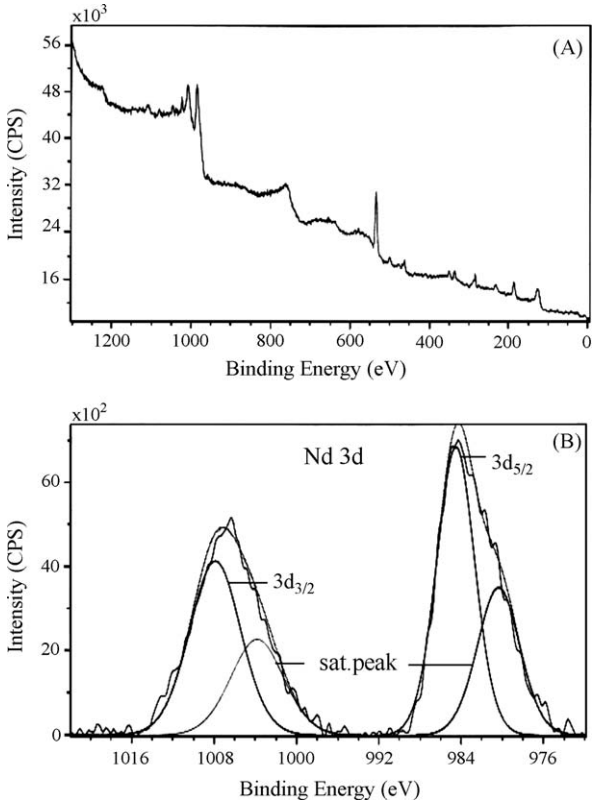

Fig. 9. XPS spectra of NZT.

Table 2
The binding energy (E in eV) of element in the Ln_2ZrTiO_7.

Element	E $d_{5/2}$	Sat. peak	E $d_{3/2}$	Sat. peak	$2p_{3/2}$	$2p_{1/2}$	Rep. value	Reference
Nd	1003.8	980.4	1007.9	984.5	–	–	980.4	[25]
Sm	1084.3	–	1111.5	–	–	–	1083.5	[45]
Zr	182.3	–	184.8	–	–	–	186.9	[42]
Ti	–	–	–	–	458.5	463.7	457.7	[42]

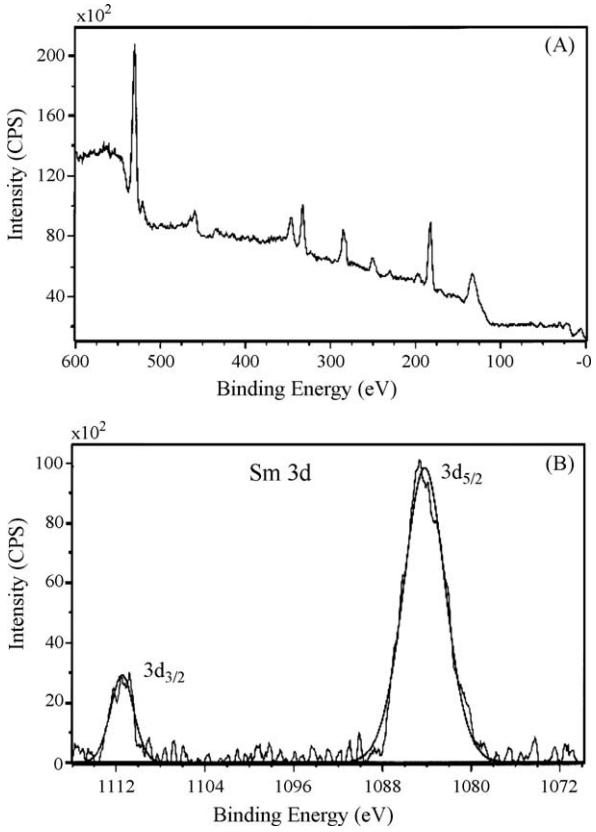

Fig. 10. XPS spectra of SZT.

O_{1s} profiles. The Ti_{2p} Gauss-fitted profile gave $2p_{3/2}$ and $2p_{1/2}$ levels at 458.55 and 463.72 eV respectively resulting a spin–orbit coupling (Δ) of 5.17 eV which is comparable to that observed in related systems [42]. Similarly, the $3d_{5/2}$ and $3d_{3/2}$ of Zr were observed at 182.3 and 184.8 eV respectively and spin–orbit coupling (Δ) was found to be 2.5 eV. The Nd_{3d} profile shows interesting features. The Nd_{3d} profiles are Gauss fitted to locate the positions of main and satellite peaks. The asymmetric $3d_{5/2}$ and $3d_{3/2}$ profiles with shoulders are Gauss fitted to locate the satellite peaks from the 3d main peaks. The satellite peaks on the low binding energy side of $3d_{5/2}$ and $3d_{3/2}$ peaks were separated by 4.12 and 4.10 eV respectively. The intensity of satellite peaks was less than that of 3d main peaks. Such broad peaks with large FWHM were attributed to

(a) a combination of life time effects and the exchange interaction between the 3d hole and partially filled 4f shell of Ln^{3+} ion [16,43] or
(b) oxidized nature of rare earth atoms [44].

According to process (a), the less intense satellites and more intense main 3d peaks are attributed to ''well screened'' $3d^9$, . . ., $4f^{n+1}$ and ''poorly screened'' $3d^9$, . . ., $4f^n$ configurations respectively. Hillerbrecht and Fuggle have interpreted the observation of satellite peaks in the XPS spectra of lanthanide compounds due to 'degree of mixing' (or hybridization) of 4f levels with extended conduction band states [16] in $LnPd_3$ (Ln = La, Ce, Pr, Nd, and Sm). It is noticed that the satellite peaks are well separated from main 3d peaks in the case of $LaPd_3$ while in $SmPd_3$ significant satellite peaks were not observed [16]. Based on the XPS spectra of these compounds, they have concluded that the degree of mixing decreases in the order La > Ce > Pr > Nd > Sm. The degree of mixing is dependent on the radial extension of 4f levels and the energy separation of dominant f^n and f^{n+1} multiplets. It was estimated that the energy difference between f^n and f^{n+1} states was found to increase from La (minimum) to Sm (maximum) [16]. According to process (b), the line shape of core-level lines is very sensitive to chemical environment/oxidation state of the core ionized atom [44]. For instance the Ce $3d_{5/2}$ profile in elemental Ce is characterized an intense ''poorly screened'' peak with negligible intensity of ''well screened'' peak while in $CePd_3$ and $CeNi_2$ the intensity of ''well screened'' peak is substantial [44] due to change in the chemical environment. All the pertinent values are given in Table 2 along with values observed in other systems.

In the present investigation the observation of satellite peaks in Nd is attributed to predominant mixing of 4f levels (process (a)) with other valence levels compared to SZT as the chemical environment/oxidation state in both the compounds is similar.

4. Conclusions

Nano sized SZT and NZT were prepared by sol–gel method. The powder XRD patterns of these materials are similar to those of $RE_2Hf_2O_7$. They were found to crystallize in cubic lattice with space group $Fd\bar{3}m$. The Raman spectra of these compounds gave characteristic bands corresponding to ''disordered pyrochlore'' structure. The morphology of SZT was found to be spherical while NZT particles were composed of spheres and platelet like objects. The photocatalytic activity of these samples was measured by the photodecomposition of methyl orange. The photoactivity was found to be less compared to that of similar systems $La_2Zr_2O_7$ and $Nd_2Zr_2O_7$ which may be due to the nature of the materials and/or less surface area due to agglomeration. The XPS spectra of NZT gave satellite peaks for Nd_{3d} levels while in SZT significant satellite peaks for Sm_{3d} were not observed. This is attributed to

the degree of mixing of 4f levels in the former and insignificant mixing of these levels in the later.

Acknowledgements

One of the authors, B.V.K., thanks the UGC and RFSMS (Research Fellowship in Science for Meritorious Students), New Delhi for providing financial support.

References

[1] M.A. Subramanian, G. Aravamudan, G.V. Subba Rao, Oxide pyrochlores – a review, Prog. Solid State Chem. 15 (2) (1983) 55–143.
[2] M.A. Subramanian, B.H. Toby, A.P. Ramirez, W.J. Marshall, A.W. Sleight, G.H. Kwei, Colossal magnetoresistance without Mn^{3+}/Mn^{4+} double exchange in the stoichiometric pyrochlore $Tl_2Mn_2O_7$, Science 273 (1996) 81–84.
[3] C.A. Mims, A.J. Jacobson, R.B. Hall, J.T. Lewandowski, Methane oxidative coupling over nonstoichiometric bismuth–tin pyrochlore catalysts, J. Catal. 153 (2) (1995) 197–207.
[4] J. Kennedy, T. Vogt, Structural and bonding trends in ruthenium pyrochlores, J. Solid State Chem. 126 (2) (1996) 261–270.
[5] S. Yonezawa, Y. Muraoka, Y. Matsushita, Z. Hiroi, Superconductivity in a pyrochlore-related oxide KOs_2O_6, J. Phys. Condens. Matter 16 (2004) L9–L12.
[6] K.W. Eberman, B.J. Wuensch, J.D. Jorgensen, Order–disorder transformations induced by composition and temperature change in $(Sc_zYb_{1-z})_2Ti_2O_7$ pyrochlores, prospective fuel cell materials, Solid State Ionics 148 (3–4) (2002) 521–526.
[7] R Vassen, X. Cao, F. Tietz, D. Basu, D. Stover, Zirconates as new materials for thermal barrier coatings, J. Am. Ceram. Soc. 83 (8) (2000) 2023–2028.
[8] S.L. Chamberlain, S.T. Hess, L.R. Corruccini, Dipolar magnetic order in the pyrochlore structure, Phys. Lett. A 323 (3–4) (2004) 310–314.
[9] N.P. Raju, M. Dion, M.J.P. Gingras, T.E. Mason, J.E. Greedan, Transition to long-range magnetic order in the highly frustrated insulating pyrochlore antiferromagnet $Gd_2Ti_2O_7$, Phys. Rev. B 59 (22) (1999) 14489–14498.
[10] N. Kim, C.P. Grey, ^{17}O MAS NMR study of the oxygen local environment in the anionic conductors $Y_2(B_{1-x}B'_x)_2O_7$ (B, B′ = Sn, Ti, Zr), J. Solid State Chem. 175 (1) (2003) 110–115.
[11] J. Lian, L.M. Wang, S.X. Wang, J. Chen, L.A. Boatner, R.C. Ewing, Nanoscale manipulation of pyrochlore: new nanocomposite ionic conductors, Phys. Rev. Lett. 87 (14) (2001), 145901-1-145901-4.
[12] F.W. Poulsen, M. Glerup, P. Holtappels, Structure, Raman spectra and defect chemistry modelling of conducting pyrochlore oxides, Solid State Ionics 135 (1–4) (2000) 595–602.
[13] P.J. Wilde, C.R.A. Catlow, Molecular dynamics study of the effect of doping and disorder on diffusion in gadolinium zirconate, Solid State Ionics 112 (3–4) (1998) 185–195.
[14] R.C. Ewing, W.J. Weber, J. Lian, Nuclear waste disposal–pyrochlore ($A_2B_2O_7$): nuclear waste form for the immobilization of plutonium and "minor" actinides, J. Appl. Phys. 95 (2004) 5949–5971.
[15] K.R. Whittle, G.R. Lumpkin, S.E. Ashbrook, Neutron diffraction and MAS NMR of cesium tungstate defect pyrochlores, J. Solid State Chem. 179 (2) (2006) 512–521.
[16] F.U. Hillerbrecht, J.C. Fuggle, Invalidity of 4f count determination and possibilities for determination of 4f hybridization in intermetallics of the light rare earths by core-levels spectroscopy, Phys. Rev. B 25 (6) (1982) 3550–3556.
[17] L.M. Falicov, W. Hanke, M.B. Maple, Valence Fluctuations in Solids, North-Holland, Amsterdam, 1981, p. 487.
[18] C.M. Varma, Mixed valence compounds, Rev. Mod. Phys. 48 (2) (1976) 219–238.
[19] M. Canpagna, G.K. Werthein, E. Bucher, Structure and Bonding, Springer, Berlin, 1976, p. 99.
[20] A.J. Signorelli, R.G. Hayes, X-ray photoelectron spectroscopy of various core levels of lanthanide ions: the roles of monopole excitation and electrostatic coupling, Phys. Rev. B 8 (1) (1973) 81–86.
[21] G.K. Wertheim, R.L. Cohen, A. Rosencwaig, H.J. Guggenheim, in: D.A. Shirley (Ed.), Electron Spectroscopy, North-Holland, Amsterdam, 1972, p. 813.
[22] C.S. Fadley, D.A. Shirley, A.J. Freeman, P.S. Bagus, J.V. Mallow, Multiplet splitting of core–electron binding energies in transition-metal ions, Phys. Rev. Lett. 23 (24) (1969) 1397–1401.
[23] H. Berthou, C.K. Jorgensen, C. Bonnelle, Influence of the ligands on 3d photoelectron spectra of the first four lanthanides, Chem. Phys. Lett. 38 (2) (1976) 199–206.
[24] J.C. Fuggle, N. Canpagna, Z. Zolnierek, R. Lasser, Observation of a relationship between core-level line shapes in photoelectron spectroscopy and the localization of screening orbitals, Phys. Rev. Lett. 45 (19) (1980) 1597–1600.
[25] A. Novosselov, E. Talik, A. Pajaczkowska, An X-ray photoelectron spectroscopy study on electron structure of some Ln-containing (Ln = La, Pr, Nd and Gd) oxide crystals, J. Alloys Compd. 351 (1–2) (2003) 50–53.
[26] R. Desai, R.V. Mehta, R.V. Upadhyay, A. Gupta, A. Praneet, K.V. Rao, Bulk magnetic properties of $CdFe_2O_4$ in nano-regime, Bull. Mater. Sci. 30 (3) (2007) 197–203.
[27] B.P. Mandal, N. Garg, S.M. Sharma, A.K. Tyagi, Preparation, XRD and Raman spectroscopic studies on new compounds $Re_2Hf_2O_7$ (Re = Dy, Ho, Er, Tm, Lu, Y): pyrochlores or defect-fluorite? J. Solid State Chem. 179 (7) (2006) 1990–1994.
[28] H. Kido, S. Komarneni, R. Roy, Preparation of $La_2Zr_2O_7$ by sol–gel route, J. Am. Ceram. Soc. 74 (2) (1991) 422–424.
[29] JCPDS Data file no. 17-0458, 1999.
[30] G.L. Catchen, T.M. Rearick, O-anion transport measured in several $R_2M_2O_7$ pyrochlores using perturbed-angular-correlation spectroscopy, Phys. Rev. B 52 (14) (1995) 9890–9899.
[31] B.P. Mandal, A. Banerji, V. Sathe, S.K. Deb, A.K. Tyagi, Order–disorder transition in $Nd_{2-y}Gd_yZr_2O_7$ pyrochlore solid solution: an X-ray diffraction and Raman spectroscopic study, J. Solid State Chem. 180 (10) (2007) 2643–2648.
[32] K.R. Whittle, L.M.D. Cranswick, S.A.T. Redfern, I.P. Swainson, G.R. Lumpkin, Lanthanum pyrochlores and the effect of yttrium addition in the systems $La_{2-x}Y_xZr_2O_7$ and $La_{2-x}Y_xHf_2O_7$, J. Solid State Chem. 182 (3) (2009) 442–450.
[33] M. Glerup, O.F. Nielsen, F.W. Poulsen, The structural transformation from the pyrochlore structure, $A_2B_2O_7$, to the fluorite structure. AO_2 studied by Raman spectroscopy and defect chemistry modeling, J. Solid State Chem. 160 (1) (2001) 25–32.
[34] F.J. Dickson, K.D. Hawkins, T.J. White, Calcium uranium titanate – a new pyrochlore, J. Solid State Chem. 82 (1) (1986) 146–150.
[35] J.M. Longo, P.M. Raccah, J.B. Goodenough, $Pb_2M_2O_7$ (M = Ru, Ir, Re) – preparation and properties of oxygen deficient pyrochlores, Mater. Res. Bull. 4 (3) (1969) 191–202.
[36] K. Koteswara Rao, M. Taqueem Banu, G.Y.S.K. Vithal, K. Swamy, Ravi Kumar, Preparation and characterization of bulk and nano particles of $La_2Zr_2O_7$ and $Nd_2Zr_2O_7$, Mater. Lett. 54 (2–3) (2002) 205–210.
[37] M.T. Vanderborre, E. Husson, J.P. Chatry, D. Michel, Rare-earth titanates and stannates of pyrochlore structure; vibrational spectra and force-fields, J. Raman Spectrosc. 14 (2) (1983) 63–71.
[38] S. Brown, H.C. Gupta, J.A. Alonso, M.J. Martinez-Lope, Vibrational spectra and force field calculation of $A_2Mn_2O_7$ (A = Y, Dy, Er, Yb), J. Raman Spectrosc. 34 (3) (2003) 240–243.
[39] M.T. Vandenborre, E. Husson, Comparison of the force field in various pyrochlore families. I. The $A_2B_2O_7$ oxides, J. Solid State Chem. 50 (3) (1983) 362–371.
[40] N.J. Hess, B.D. Begg, S.D. Conradson, D.E. McCready, P.L. Gassman, W.J. Weber, Spectroscopic investigations of the structural phase transition in $Gd_2(Ti_{1-y}Zr_y)_2O_7$ pyrochlores, J. Phys. Chem. B 106 (18) (2002) 4663–4677.
[41] Y. Tong, J. Zhu, L. Lu, X. Wang, X. Yang, Preparation and characterization of $Ln_2Zr_2O_7$ (Ln = La and Nd) nanocrystals and their photocatalytic properties, J. Alloys Compd. 465 (1–2) (2008) 280–284.

[42] J. Wang, Z.G. Wu, X.M. Yuan, S.R. Jiang, P.X. Yan, The effect of heat-treatment on the structure and chemical homogeneity of ferroelectrics PLZT thin films deposited by R.F. sputtering, Mater. Chem. Phys. 88 (1) (2004) 77–83.

[43] J.C. Fuggle, S.F. Alvarado, Core-level lifetimes as determined by X-ray photoelectron spectroscopy measurements, Phys. Rev. A 22 (4) (1980) 1615–1624.

[44] J.C. Fuggle, M. Campagna, Z. Zolnierek, R. Lasser, A. Platau, Observation of a relationship between core-level line shapes in photoelectron spectroscopy and the localization of screening orbitals, Phys. Rev. Lett. 45 (19) (1980) 1597–1600.

[45] D. Briggs, M.P. Seah (Eds.), Practical Surface Analysis by Auger and X-ray Photoelectron Spectroscopy, John Wiley & Sons, New York, 1987, p. 51.